

Chapter 2

Experimental Dynamic Substructuring of the Ampair Wind Turbine Test Bed

Jacopo Brunetti, Antonio Culla, Walter D'Ambrogio, and Annalisa Fregolent

Abstract In a recent paper, the authors discussed the selection of a reduced set of interface DoFs in order to describe the coupling between the blades and the hub of the Ampair test bed wind turbine rotor. The study was conducted using simulated FRFs obtained from Finite Element model of the blades and the hub, but in view of using experimental FRFs. In this paper, test data measured on the turbine by the UW-Madison participants in the IMAC Focus Group on Experimental Dynamic Substructuring, and posted on the Wiki page of the group, are used for dynamic substructuring of the wind turbine test bed.

Keywords Experimental dynamic substructuring • Wind turbine • Modal identification • Frequency response function synthesis • Frequency based substructuring

2.1 Introduction

Experimental Dynamic Substructuring is a very powerful tool in the analysis of dynamic behavior of complex mechanical systems and responds to actual industrial needs. Two main problem can be defined that allow to perform the addition (coupling) and the subtractions (decoupling) of substructures.

In experimental contexts, coupling techniques allow to estimate the dynamic response of a complex structure that cannot be tested in one piece while the model of the component systems can be derived from experimental tests. On the contrary, decoupling techniques can be useful in complete structures where some components cannot be accessed easily or when some components cannot be removed and tested separately.

Addition of substructures (coupling) can be seen as a structural modification problem [1]. Similarly, the decoupling problem can be seen as a structural modification problem with negative modification. Due to modal truncation problems, in experimental dynamic substructuring, the use of FRFs (Frequency Based Substructuring) can be preferred with respect to the use of modal parameters. The main algorithm for frequency based substructuring is the improved impedance coupling [2] that involves just one matrix inversion with respect to the classical impedance coupling technique that requires three inversions. A general framework for dynamic substructuring is provided in [3,4]: in this context, the so called dual domain decomposition is very useful for experimental application, since it allows to retain the full set of global DoFs by ensuring equilibrium at the interface between substructures. A similar formulation for the decoupling problem is developed and discussed in [5–7].

J. Brunetti

Dipartimento di Ingegneria Industriale e dell'Informazione e di Economia, Università dell'Aquila, Via G. Gronchi, 18
I-67100 L'Aquila (AQ), Italy

LaMCos, Contacts and Structural Mechanics Laboratory, Université de Lyon, CNRS, INSA-Lyon, UMR 5259, rue des Sciences, 69621
Villeurbanne, France

A. Culla • A. Fregolent

Dipartimento di Ingegneria Meccanica e Aerospaziale, Università di Roma La Sapienza, Via Eudossiana 18, I 00184 Rome, Italy

W. D'Ambrogio (✉)

Dipartimento di Ingegneria Industriale e dell'Informazione e di Economia, Università dell'Aquila, Via G. Gronchi, 18
I-67100 L'Aquila (AQ), Italy
e-mail: walter.dambrogio@univaq.it

In this paper, dynamic substructuring is applied to the Ampair 600 wind turbine. This system has been proposed as a test bed by the Society of Experimental Mechanics focus group on experimental dynamic substructuring, to enable advancements in experimental dynamic substructuring technology and theory. Several specimens of the turbine have been bought by some participants in the focus group. A description of the turbine with modifications made to the system to make it more linear is presented in [8] together with results from a rudimentary modal test on the whole turbine. In a recent paper [9], the authors discussed the selection of a reduced set of interface DoFs in order to describe the coupling between the blades and the hub of the Ampair test bed wind turbine rotor. The study was conducted using simulated FRFs obtained from Finite Element model of the blades and the hub, but in view of using experimental FRFs.

The experimental FRFs used in this paper are measured by UW-Madison on the full turbine, on the two-bladed turbine and on a mass-loaded bladed, and are posted on the Wiki page of the IMAC Experimental Dynamics Substructuring Focus Group. Curve fitting of raw measured FRFs is performed after a reciprocity analysis aimed to select the more convenient reference DoFs, using a poly-reference Least Square Frequency Domain technique. Since some unmeasured FRFs are required to apply the coupling procedure, they are synthesized using the identified modal parameters. Finally, the results of substructuring are presented and discussed.

2.2 Coupling and Decoupling in the Frequency Domain

The coupled structural system is assumed to be made by two (or more) subsystems joined through a number of couplings (see Fig. 2.1). The degrees of freedom (DoFs) of the coupled system can be partitioned into internal DoFs (not belonging to the couplings) and coupling DoFs.

2.2.1 Addition of Subsystems

If addition of subsystems (coupling problem) is considered, all subsystems are assumed to be known whilst the FRF of the coupled system is unknown. In the frequency domain, the equation of motion of a linear time-invariant subsystem r may be written as:

$$[Z^{(r)}(\omega)] \{u^{(r)}(\omega)\} = \{f^{(r)}(\omega)\} + \{g^{(r)}(\omega)\} \quad (2.1)$$

where:

- $[Z^{(r)}]$ is the dynamic stiffness matrix of subsystem r ;
- $\{u^{(r)}\}$ is the vector of degrees of freedom of subsystem r ;
- $\{f^{(r)}\}$ is the external force vector;
- $\{g^{(r)}\}$ is the vector of connecting forces with other subsystems (constraint forces arising from compatibility conditions).

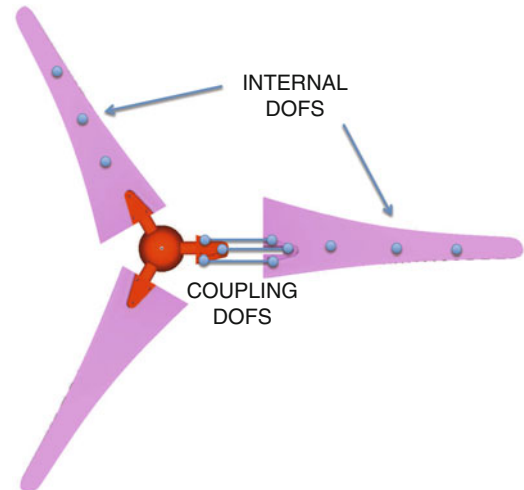


Fig. 2.1 Scheme of the substructuring problem

For the sake of simplicity, the explicit frequency dependence will be omitted. Furthermore, the procedure will be developed with reference to two subsystems, bearing in mind that it can be easily extended to more subsystems.

The equation of motion of the subsystems to be coupled can be written in a block diagonal format as:

$$[Z]\{u\} = \{f\} + \{g\} \quad \text{i.e.} \quad \begin{bmatrix} [Z^{(1)}] & [0] \\ [0] & [Z^{(2)}] \end{bmatrix} \begin{Bmatrix} \{u^{(1)}\} \\ \{u^{(2)}\} \end{Bmatrix} = \begin{Bmatrix} \{f^{(1)}\} \\ \{f^{(2)}\} \end{Bmatrix} + \begin{Bmatrix} \{g^{(1)}\} \\ \{g^{(2)}\} \end{Bmatrix} \quad (2.2)$$

The compatibility condition at the interface DoFs implies that any pair of matching DoFs $u_l^{(1)}$ and $u_m^{(2)}$, i.e. DoF l on subsystem 1 and DoF m on subsystem 2 must have the same displacement, that is $u_l^{(1)} - u_m^{(2)} = 0$.

This condition can be generally expressed as:

$$[B]\{u\} = \{0\} \quad \text{i.e.} \quad \begin{bmatrix} [B^{(1)}] & [B^{(2)}] \end{bmatrix} \begin{Bmatrix} \{u^{(1)}\} \\ \{u^{(2)}\} \end{Bmatrix} = \{0\} \quad (2.3)$$

where each row of $[B]$ corresponds to a pair of matching DoFs. Note that $[B]$ is, in most cases, a signed Boolean matrix and it can be written by distinguishing the contribution of the different subsystems.

The equilibrium condition for constraint forces associated with the compatibility conditions implies that, when the connecting forces are added for a pair of matching DoFs, their sum must be zero, i.e. $g_l^{(1)} + g_m^{(2)} = 0$: this holds for any pair of matching DoFs. Furthermore, if DoF k on subsystem 1 (or 2) is not a connecting DoF, it must be $g_k^{(1)} = 0$: this holds for any non-interface DoF.

Overall, the above conditions can be expressed as:

$$[L]^T \{g\} = \{0\} \quad (2.4)$$

where the matrix $[L]$ is a Boolean localisation matrix. Note that the number of rows of $[L]^T$ is equal to the number of non-interface DoFs plus the number of pairs of interface DoFs.

Equations (2.2)–(2.4) can be put together to obtain the so called 3-field formulation [3]:

$$\begin{cases} [Z]\{u\} = \{f\} + \{g\} \\ [B]\{u\} = \{0\} \\ [L]^T \{g\} = \{0\} \end{cases} \quad (2.5)$$

2.2.1.1 Dual Formulation in the Frequency Domain [3]

In the dual formulation, the total set of DoFs is retained, i.e. each interface DoF is present as many times as there are substructures connected through that DoF. The equilibrium condition $g_l^{(1)} + g_m^{(2)} = 0$ at a pair of interface DoFs is ensured by choosing, for instance, $g_l^{(1)} = -\lambda$ and $g_m^{(2)} = \lambda$. Due to the construction of $[B]$, the overall interface equilibrium can be ensured by writing the connecting forces in the form:

$$\{g\} = -[B]^T \{\lambda\} \quad (2.6)$$

where $\{\lambda\}$ are Lagrange multipliers corresponding to connecting force intensities. Since there is a unique set of connecting force intensities λ , the interface equilibrium condition Eq. (2.4) is satisfied automatically for any λ , i.e.

$$[L]^T \{g\} = -[L]^T [B]^T \{\lambda\} = \{0\} \quad (2.7)$$

Then $[B]^T$ is the nullspace of $[L]^T$, so Eq. (2.7) is always satisfied and the system of Eq. (2.5) becomes:

$$\begin{cases} [Z]\{u\} + [B]^T \{\lambda\} = \{f\} \\ [B]\{u\} = \{0\} \end{cases} \quad (2.8)$$

In matrix notation:

$$\begin{bmatrix} [Z] & [B]^T \\ [B] & [0] \end{bmatrix} \begin{Bmatrix} \{u\} \\ \{\lambda\} \end{Bmatrix} = \begin{Bmatrix} \{f\} \\ \{0\} \end{Bmatrix} \quad (2.9)$$

that is:

$$\begin{bmatrix} [Z^{(1)}] & [0] & [B^{(1)}]^T \\ [0] & [Z^{(2)}] & [B^{(2)}]^T \\ [B^{(1)}] & [B^{(2)}] & [0] \end{bmatrix} \begin{Bmatrix} \{u^{(1)}\} \\ \{u^{(2)}\} \\ \{\lambda\} \end{Bmatrix} = \begin{Bmatrix} \{f^{(1)}\} \\ \{f^{(2)}\} \\ \{0\} \end{Bmatrix} \quad (2.10)$$

Note that $[B^{(1)}]$ and $[B^{(2)}]$ extract the coupling DoFs among the full set of DoFs.

By eliminating $\{\lambda\}$, it is possible to obtain a relation in the form $\{u\} = [H]\{f\}$, which provides the FRF of the coupled system [6]:

$$\{u\} = \left([Z]^{-1} - [Z]^{-1} [B]^T ([B] [Z]^{-1} [B]^T)^{-1} [B] [Z]^{-1} \right) \{f\} \quad (2.11)$$

In expanded notation:

$$\begin{aligned} \begin{Bmatrix} \{u^{(1)}\} \\ \{u^{(2)}\} \end{Bmatrix} &= \left(\begin{bmatrix} [Z^{(1)}] & [0] \\ [0] & [Z^{(2)}] \end{bmatrix}^{-1} - \begin{bmatrix} [Z^{(1)}] & [0] \\ [0] & [Z^{(2)}] \end{bmatrix}^{-1} \begin{bmatrix} [B^{(1)}]^T \\ [B^{(2)}]^T \end{bmatrix} \right. \\ &\quad \times \left(\begin{bmatrix} [B^{(1)}] & [B^{(2)}] \end{bmatrix} \begin{bmatrix} [Z^{(1)}] & [0] \\ [0] & [Z^{(2)}] \end{bmatrix}^{-1} \begin{bmatrix} [B^{(1)}]^T \\ [B^{(2)}]^T \end{bmatrix} \right)^{-1} \\ &\quad \left. \times \begin{bmatrix} [B^{(1)}] & [B^{(2)}] \end{bmatrix} \begin{bmatrix} [Z^{(1)}] & [0] \\ [0] & [Z^{(2)}] \end{bmatrix}^{-1} \right) \begin{Bmatrix} \{f^{(1)}\} \\ \{f^{(2)}\} \end{Bmatrix} \end{aligned} \quad (2.12)$$

i.e., by introducing the FRFs $[H^{(1)}]$ and $[H^{(2)}]$ at the full set of DoFs instead of $[[Z^{(1)}]]^{-1}$ and $[[Z^{(2)}]]^{-1}$:

$$\begin{aligned} [H^{RU}] &= \begin{bmatrix} [H^{(1)}] & [0] \\ [0] & [H^{(2)}] \end{bmatrix} - \begin{bmatrix} [H^{(1)}] & [0] \\ [0] & [H^{(2)}] \end{bmatrix} \begin{bmatrix} [B^{(1)}]^T \\ [B^{(2)}]^T \end{bmatrix} \\ &\quad \times \left(\begin{bmatrix} [B^{(1)}] & [B^{(2)}] \end{bmatrix} \begin{bmatrix} [H^{(1)}] & [0] \\ [0] & [H^{(2)}] \end{bmatrix} \begin{bmatrix} [B^{(1)}]^T \\ [B^{(2)}]^T \end{bmatrix} \right)^{-1} \begin{bmatrix} [B^{(1)}] & [B^{(2)}] \end{bmatrix} \begin{bmatrix} [H^{(1)}] & [0] \\ [0] & [H^{(2)}] \end{bmatrix} \end{aligned} \quad (2.13)$$

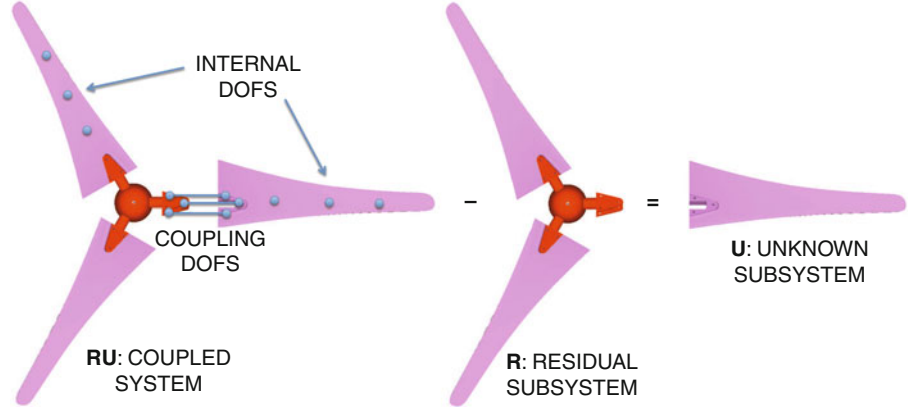
With the dual formulation, the rows and columns corresponding to the coupling DoFs appear twice in $[H^{RU}]$. Obviously, only independent entries are retained.

2.2.2 Subtraction of Subsystems Using the Dual Domain Decomposition [6]

If subtraction of subsystems (decoupling problem) is considered, the coupled structural system RU and a residual subsystem R are assumed to be known whilst the FRF of subsystem U is unknown. The unknown subsystem U and the residual subsystem R are joined through a number of couplings (see Fig. 2.2). The degrees of freedom (DoFs) of the coupled system can be partitioned into internal DoFs (u) of subsystem U (not belonging to the couplings), internal DoFs (r) of subsystem R , and coupling DoFs (c).

It is required to find the FRF of the unknown substructure U starting from the FRF of the coupled system RU . The subsystem U can be extracted from the coupled system RU by canceling the dynamic effect of the residual subsystem R . This can be accomplished by adding to the coupled system RU a fictitious subsystem with a dynamic stiffness opposite to that of the residual subsystem R and satisfying compatibility and equilibrium conditions. According to this point of view, the interface between the coupled system RU and the fictitious subsystem should not only include the coupling DoFs between

Fig. 2.2 Scheme of the decoupling problem



subsystems U and R , but should as well include the internal DoFs of subsystem R . However, it can be shown that the problem can be solved by considering a number of interface DoFs at least equal to the number of coupling DoFs n_c . Therefore, three options for interface DoFs can be considered:

- standard interface, including only the coupling DoFs (c) between subsystems U and R ;
- extended interface, including also some internal DoFs ($i \subseteq r$) of the residual substructure;
- mixed interface, including some coupling DoFs ($d \subseteq c$) and/or some internal DoFs ($i \subseteq r$) of the residual substructure.

In the framework of the dual formulation in the frequency domain (see Sect. 2.2.1.1), the union between the coupled system RU and the fictitious subsystem can be written (see Eq. (2.10)) as:

$$\begin{bmatrix} [Z^{RU}] & [0] & [B_E^{RU}]^T \\ [0] & -[Z^R] & [B_E^R]^T \\ [B_C^{RU}] & [B_C^R] & [0] \end{bmatrix} \begin{Bmatrix} \{u^{RU}\} \\ \{u^R\} \\ \{\lambda\} \end{Bmatrix} = \begin{Bmatrix} \{f^{RU}\} \\ \{f^R\} \\ \{0\} \end{Bmatrix} \quad (2.14)$$

Following the same procedure used in Sect. 2.2.1.1, it is possible to obtain the FRF of the unknown subsystem U .

$$\begin{aligned} [H^U] &= \begin{bmatrix} [H^{RU}] & [0] \\ [0] & -[H^R] \end{bmatrix} - \begin{bmatrix} [H^{RU}] & [0] \\ [0] & -[H^R] \end{bmatrix} \begin{bmatrix} [B_E^{RU}]^T \\ [B_E^R]^T \end{bmatrix} \\ &\quad \times \left(\begin{bmatrix} [B_C^{RU}] & [B_C^R] \end{bmatrix} \begin{bmatrix} [H^{RU}] & [0] \\ [0] & -[H^R] \end{bmatrix} \begin{bmatrix} [B_E^{RU}]^T \\ [B_E^R]^T \end{bmatrix} \right)^{-1} \begin{bmatrix} [B_C^{RU}] & [B_C^R] \end{bmatrix} \begin{bmatrix} [H^{RU}] & [0] \\ [0] & -[H^R] \end{bmatrix} \end{aligned} \quad (2.15)$$

Note that $[H^{RU}]$ and $[H^R]$ are the FRFs at the full set of DoFs of the coupled system and the residual subsystem.

2.3 Test Structure

In this paper the dynamic behavior of the Ampair 600 wind turbine is analyzed. The rotor is composed by three blades clamped to the hub by three bolt and two aluminum plates that sandwich each blade. The rotor is positioned at the top of an aluminum pole fixed on a heavy basement. The whole structure is supported on an elastic trampoline during experimental tests.

Blades are made of glass reinforced polyester and they are coated with a white epoxy. Internal components of the rotor are eliminated and replaced by a dummy mass. The cavity of the hub is filled by a potting material to fix all the components and block the pitch mechanism of the blades.

Non-linearities of composite materials are very hard to model numerically and experimental characterization is the best way to obtain a reliable representation of the dynamic behavior of the blade.

In this paper two substructures are considered to solve the coupling problem. The first subsystem is the blade and the other substructure is the turbine without a blade. Experimental data of the two subsystems are provided by the University of Wisconsin—Madison and can be coupled by means of frequency based substructuring to find the behavior of the whole system.

2.4 Experimental Dynamic Substructuring

In this section the results of experimental dynamic substructuring performed on the Ampair Wind turbine are reported. The dynamic behavior of the whole system is predicted by coupling the mass loaded blade and the two bladed turbine subsystems by means of the Frequency Based Substructuring technique. The predicted FRFs are compared with those measured on the assembled system.

2.4.1 Experimental Data Description

The experimental data used for this substructuring are the data shared by the University of Wisconsin—Madison on the Wiki of the substructuring focus group, acquired on the mass loaded blade and on the two bladed turbine.

Data provided for the mass loaded blade are acceleration FRFs (inertances) measured over three response DoFs by accelerometers placed at two different points (on the tip and on the root of the blade) and for 59 different excitation DoFs, roving the instrumented hammer over 27 points along different directions (Fig. 2.3a). Three nodes are located in correspondence with the three bolts used to fix the blade to the rest of the structure (nodes 16, 17, 18) and excitations are applied on the three spatial directions for each of the three nodes.

A mass-load is applied on the mounting interface of the blade to simulate how the blade is held by the wind turbine. This mass is composed by a block of steel sandwiched between two aluminum plates. This mass results to be rigid in the frequency range of interest. Starting from the pictures published on the wiki internet site, a solid model of the mass is built and inertial characteristics (mass and moments of inertia) are calculated.

The experimental data used to characterize the two-bladed turbine subsystem are measured on three points with bi-axial accelerometers. Excitations are applied by an instrumented hammer over 94 DoFs placed on 51 different points. Also in this case, three nodes are placed in correspondence with the coupling interface and excitations are applied on the nine translational DoFs (Fig. 2.3b).

The dynamic response of the whole turbine is obtained coupling the two subsystems and canceling the load mass effect from the coupled structure.

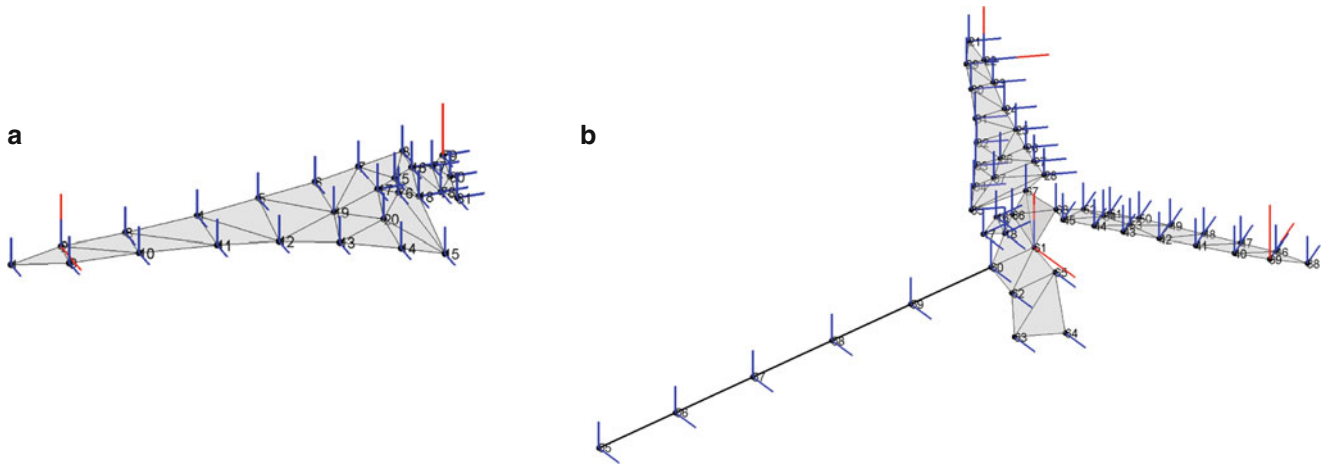


Fig. 2.3 Nodes and directions of the measured data. — excitation DoFs; — response DoFs. (a) Measured inertances on the mass loaded blade subsystem. (b) Measured inertances on the 2 bladed turbine subsystem (Color figure online)

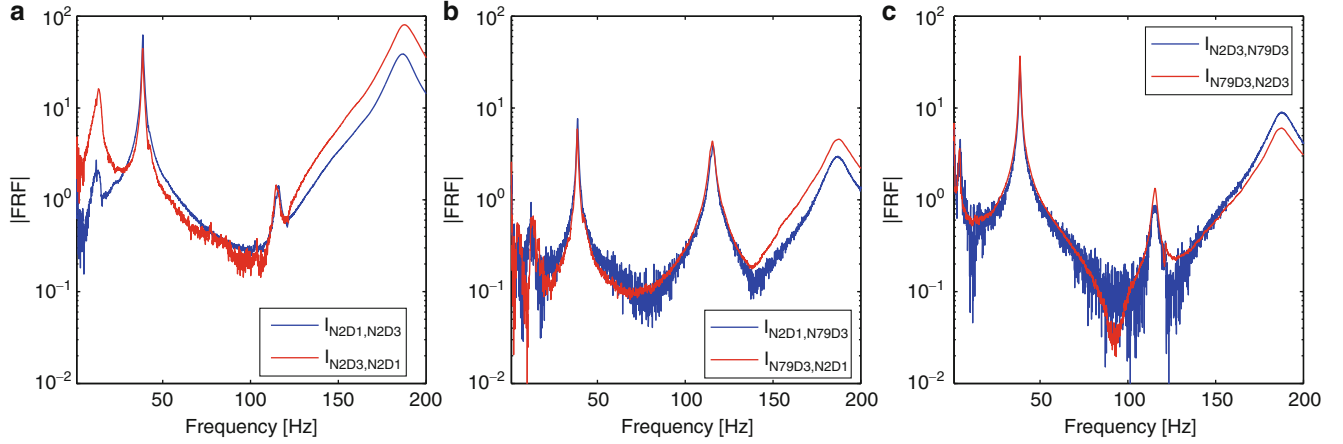


Fig. 2.4 Reciprocal terms of the measured Inertance Matrix for the blade subsystem. (a) FRFs between 2x-2z. (b) FRFs between 2x-79z. (c) FRFs between 2z-79z (Color figure online)

2.4.2 Response Selection and Curve Fitting

From a preliminary observation of the experimental data (Figs. 2.4 and 2.5), it appears that there is a lack of coherence between some of the reciprocal terms of the inertance matrix that are expected to be equal. Two series of results have been considered to perform the modal identification of the blade. Data selected for modal identification are data measured on the node 2 and 79 in the third local direction (Fig. 2.4c).

The same problem is encountered on the two bladed turbine subsystem (Fig. 2.5c, e, f) and a reduced set of the measured FRFs is selected to guarantee that reciprocal terms of the inertance matrix are almost equal. The subset selected for modal identification is composed by response data on nodes 22, 39 and 61 in the local x direction (Fig. 2.5a, b, d).

Modal identification is performed by means of Poly-Reference Least Square Complex Frequency Domain (Poly-LSCF) optimized to guarantee the symmetry of the residue matrix [10].

FRFs are defined for several excitation DoFs and a few response DoFs. The experimental inertance matrix is a rectangular matrix of size $n \times m$ where n is the number of response DoFs and $m > n$ is the number of excited DoFs. For the use of Poly-LSCF method the transposed matrix is considered where n is the number of references and m is the number of outputs of the poly-reference method.

Figure 2.6a shows the stabilization plot for the mass loaded blade in the frequency range 0–150 Hz for a model order in the range 20–50. Modes below 20 Hz correspond to the suspension system of the blade adopted for experimental tests but they are considered in the curve fitting in order to account for the effects of rigid body modes in the synthesis of unmeasured FRFs (see Sect. 2.4.3). Figure 2.6b shows the result of modal identification for the selected model order 34 highlighting a good quality of curve fitting of the experimental data both in amplitude and in phase for the blade subsystem. The modal identification shows two main modes of the mass loaded blade at 38 and 115 Hz. Other modes are found that are not physical modes of the blade but are necessary to fit the experimental responses.

Figure 2.7a shows the stabilization plot for the two bladed turbine subsystem in the frequency range 1–150 Hz for a model order in the range 40–80. The two bladed turbine subsystem presents a very complex dynamic behavior in the considered range. Figure 2.7b shows the curve fitting results for the selected model order 77 highlighting also in this case a good agreement between experimental and fitted data.

2.4.3 Synthesis of the Unmeasured FRF Elements

Substructuring techniques in the frequency domain need the knowledge of the complete (square) Frequency Response matrix of the two substructures to couple at least in the coupling DoFs (Eq. (2.13)).

Experimental data fitted by means of Poly-LSCF method provide in this case a rectangular FRF matrix (having the same size of the transposed experimental inertance matrix). The identification of modal parameters provides for each mode r the eigenvector $\{\psi\}_r$ having the same length m of output DoFs, the modal participation factors $\{\tilde{L}\}_r$ having the same length n of reference DoFs and the eigenvalue λ_r . In experimental data $n < m$ and the vector of modal participation is incomplete.

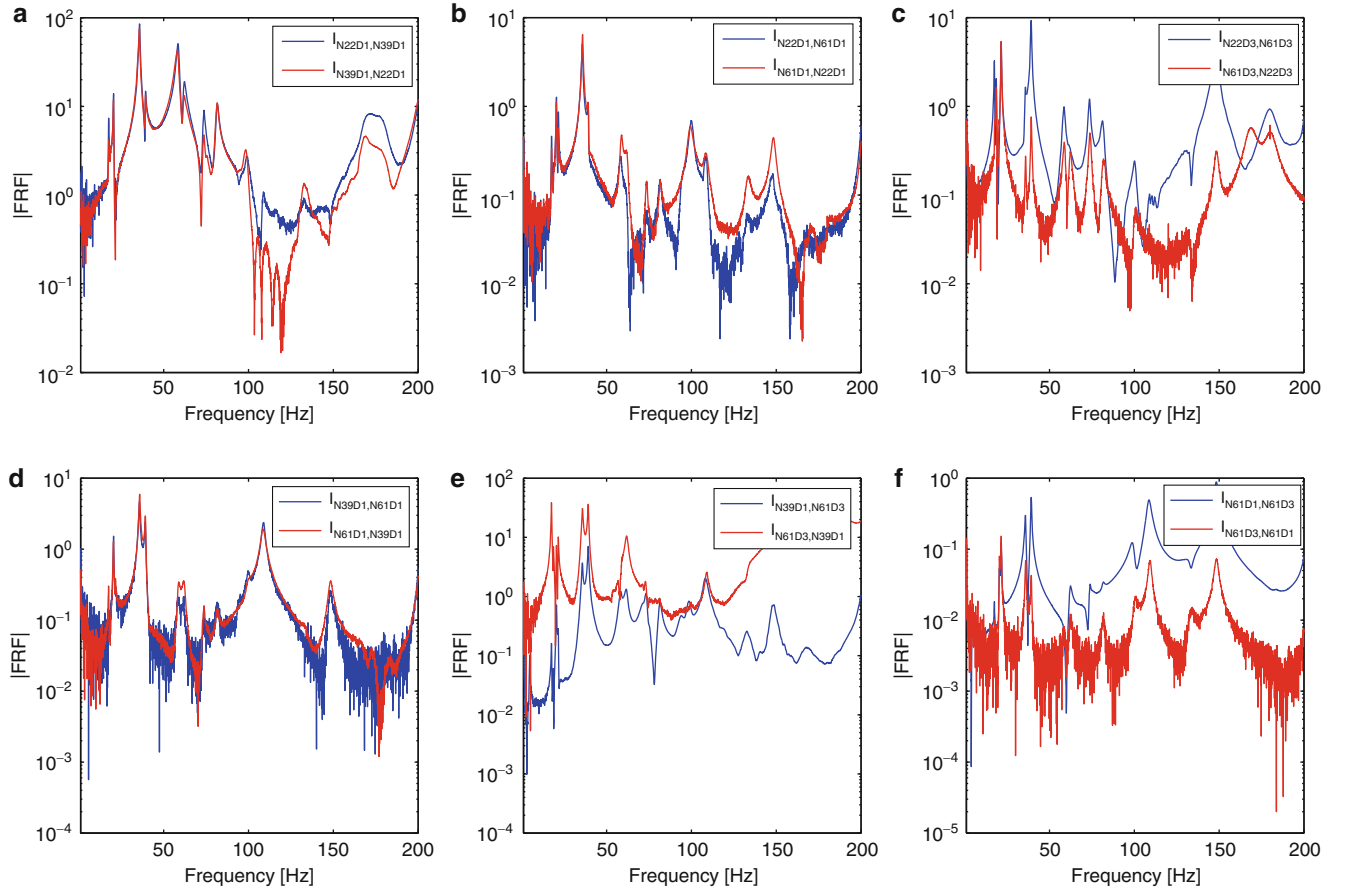


Fig. 2.5 Reciprocal terms of the measured inertance matrix for the two bladed turbine subsystem. (a) FRFs between 22x-39x. (b) FRFs between 22x-61x. (c) FRFs between 22z-61z. (d) FRFs between 39x-61x. (e) FRFs between 39x-61z. (f) FRFs between 61x-61z (Color figure online)

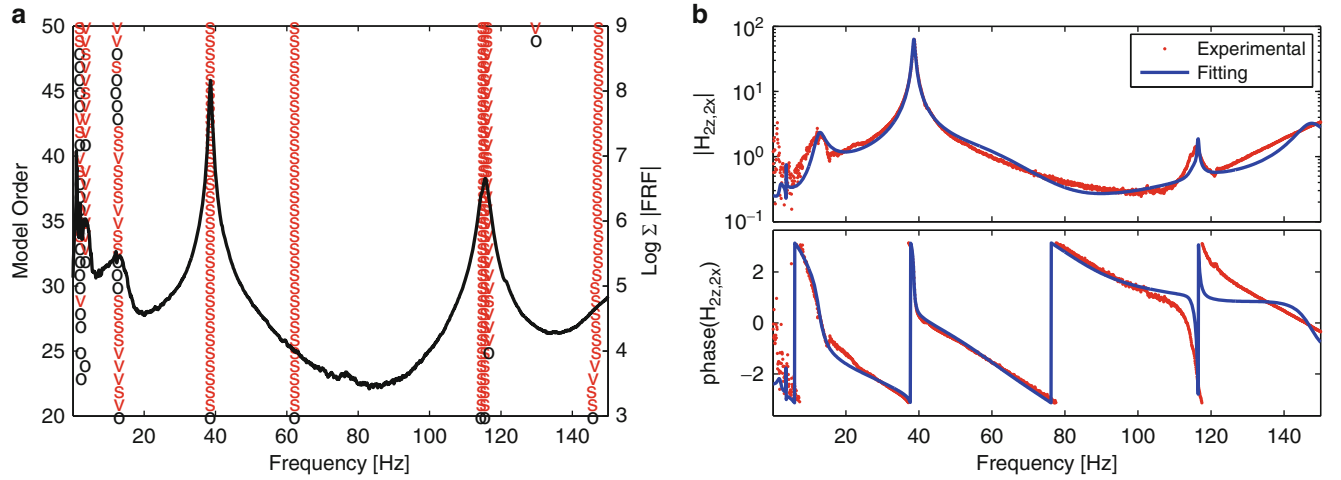


Fig. 2.6 Modal identification of the mass loaded blade subsystem. (a) Stabilization plot of the Ploy-LSCF. (b) Identification results

From the theory, the complete vector of modal participation factors $\{L\}_r$ is proportional to the corresponding eigenvector $\{\psi\}_r$. For each reference DoF n , a complex proportionality constant c_n can be defined as:

$$c_n = \frac{\tilde{L}_{n,r}}{\psi_{n,r}} \quad (2.16)$$

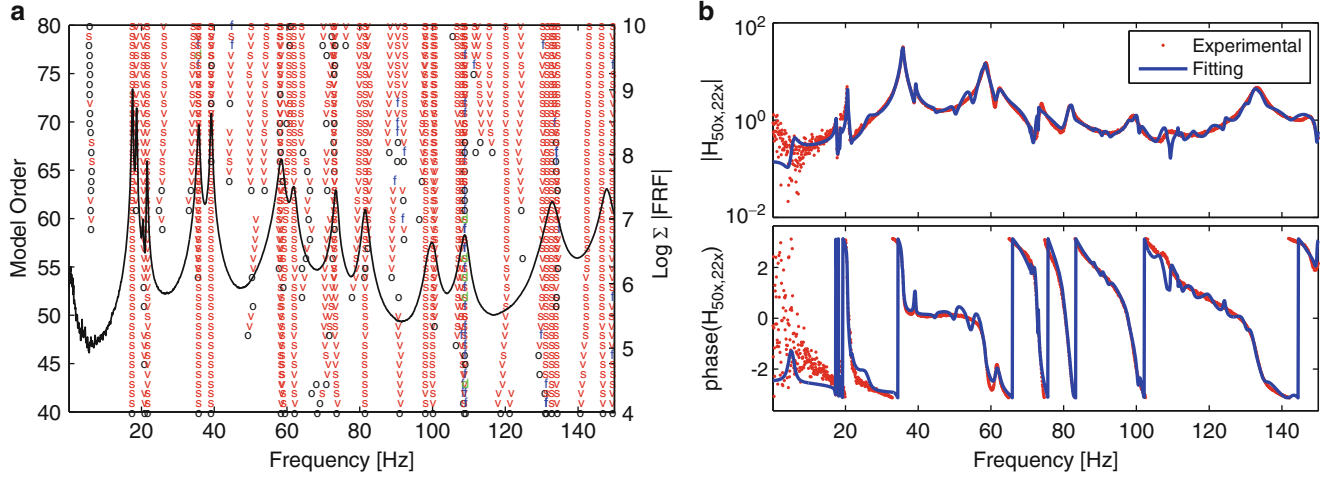


Fig. 2.7 Modal identification of the two bladed turbine subsystem. (a) Stabilization plot of the Poly-LSCF. (b) Identification results

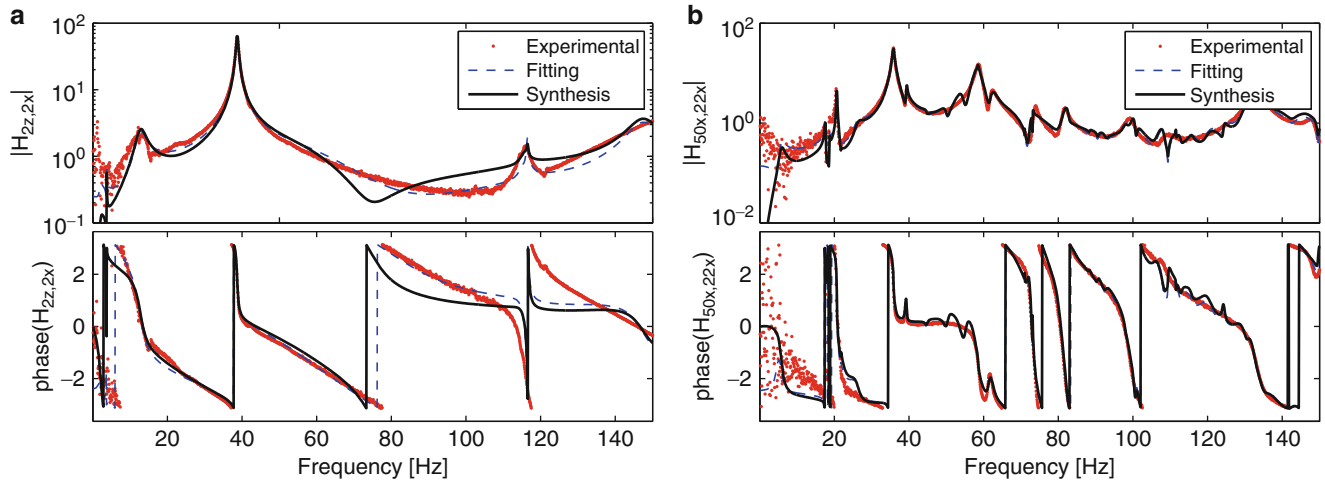


Fig. 2.8 Comparison between experimental, fitted and synthesized FRFs. (a) Mass loaded blade subsystem. (b) Two bladed turbine subsystem

and an average value c can be used to find the r -th modal participation vector as:

$$\{L\}_r = c \{\psi\}_r \quad (2.17)$$

Finally, the full matrix of FRFs (inertances) defined also on unmeasured DoFs can be expressed as:

$$[H(i\omega)] = -\omega^2 \sum_{r=1}^n \left(\frac{\{\psi\}_r \{L\}_r^T}{i\omega - \lambda_r} + \frac{\{\psi\}_r^* \{L\}_r^{T*}}{i\omega - \lambda_r^*} \right) \quad (2.18)$$

In this case, due to the complexity, to the high nonlinearity of the dynamic behavior of the system and to the lack of coherence between different measurement, it can be more convenient to select a single proportionality constant rather than to average the different proportionality constants on all the reference DoFs.

For the mass loaded blade subsystem, the proportionality constant used to compute the participation vectors is the one corresponding to the reference DoF on Node 2 in x local direction. For the two bladed turbine the selected DoF used to compute the proportionality constant is the one corresponding to node 22 on the x local direction.

The response synthesized according to Eq. (2.18) are reported in Fig. 2.8. Below 15 Hz, the absence of low frequency residuals, that are taken into account in the curve fitting but cannot be considered in the synthesized FRFs, produces a relevant error. Synthesized FRFs are quite reliable for frequency higher than 15 Hz.

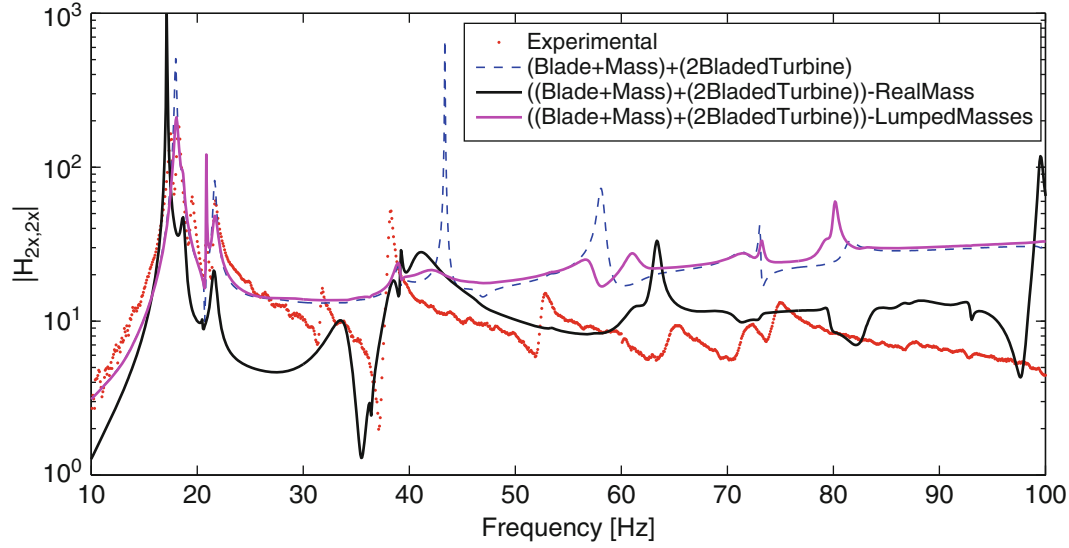


Fig. 2.9 Experimental (*** vs. predicted FRF of the coupled structure: without cancellation of the added mass (---); with cancellation of the added mass modeled by 3 lumped masses (—) or by a rigid body (—) (Color figure online)

2.4.4 Coupling of the Blade with the Two Bladed Turbine and Mass Cancellation

The subsystems identified in the previous section are here used to perform the coupling operation in the frequency domain. To find the dynamic response of the whole system the mass loaded blade is first coupled with the two bladed turbine and then the mass is subtracted from the whole structure by a decoupling operation.

Coupling DoFs are those on nodes 16, 17, 18 along the three spatial directions. The corresponding FRFs are synthesized according to Eq. (2.18). The equilibrium and compatibility conditions are defined for all nine coupling DoFs. The effect of the mass added to the blade can be subsequently canceled by a decoupling operation. The loading mass was initially modeled by three lumped masses placed at the coupling nodes. In this case, the inertance matrix can be expressed as a diagonal matrix with the element on the main diagonal equal to $3/m$ where m is the total added mass. The added mass is also modeled as a continuous rigid body, using a consistent mass matrix that takes into account static and inertia moments of the body.

Figure 2.9 shows the FRF of the assembled system, resulting from preliminarily coupling the two substructures and subsequently decoupling the loading mass, compared with the experimental FRF, both referred to node 2 in x local direction. The predicted FRF computed by decoupling the added mass, modeled using a consistent mass matrix, reproduces the experimental response globally better than the FRF computed by decoupling the model with three lumped masses. However, the decoupling of the lumped masses shows a more faithful reproduction of the experimental behavior for frequencies lower than 30 Hz.

To discuss this difference, we can analyze the FRFs predicted at points that are far from the coupling interface, after coupling the two substructures. It can be noticed that the coupling operation doesn't substantially modify the FRFs: Figure 2.10 shows the FRFs of the substructures before and after the coupling procedure for an internal DoF (node 9 in z local direction) of the mass loaded blade (Fig. 2.10a) and for an internal DoF (node 36 in z local direction) of the two bladed turbine substructure (Fig. 2.10b). Below 60 Hz, the FRFs before and after coupling are similar in both cases, whilst a substantial variation of the response amplitude can be noticed for the mass loaded blade at frequencies higher than 60 Hz. It can be concluded that in the low frequency range the two substructures have an almost independent dynamic behavior. Therefore, it is preferable to obtain a low error above 40 Hz as provided by the consistent mass model (Fig. 2.9).

2.5 Conclusions

In this paper, the dynamic response of a complex structure, the Ampair 600 test bed wind turbine, is predicted by a Frequency Based Substructuring technique. The dynamic behavior of the assembled Ampair turbine is obtained by coupling the mass-loaded blade with the two-bladed turbine, and subsequently canceling the contribution of the added mass. The experimental

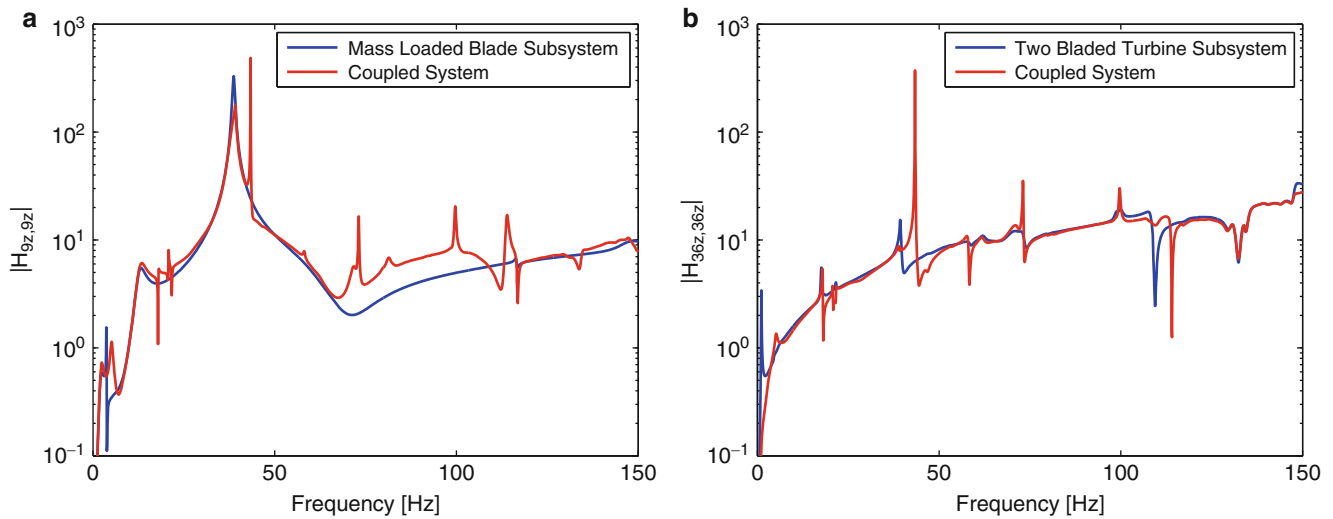


Fig. 2.10 Predicted FRF of the coupled system (—) vs. synthesized FRF of the component substructures (—) at two internal DoFs of the component substructures. (a) Effect of coupling on the mass loaded blade. (b) Effect of coupling on the two bladed turbine (Color figure online)

data used for substructuring are the inertances measured over a set of excitation and response DoFs. These data are shared by the University of Wisconsin-Madison.

Due to the lack of coherence between some reciprocal terms of the inertance matrix, Poly-LSCF modal identification is applied using a reduced set of reference DoFs. The comparison between the measured and the fitted FRFs shows a good agreement in the frequency range up to 150 Hz.

Substructuring techniques in the frequency domain need the complete FRFs matrix at the coupling DoFs. Since the available measurements do not include all the required FRFs, a consistent FRF matrix is synthesized using the identified modal parameters. Synthesized FRFs are quite reliable for frequencies higher than 15 Hz. Below 15 Hz, the lack of low frequency residuals, that are considered in the curve fitting but can not be included in the synthesizing procedure, produces some error.

The predicted FRF of the assembled structure, obtained by coupling the mass-loaded blade with the two-bladed turbine, and subsequently decoupling the added mass, modeled as a continuous rigid body, shows an acceptable agreement with the tests. Of course, the complexity of the structure must be considered together with the challenging task of synthesizing good FRFs from measurements. At frequencies below 30 Hz, the predicted FRF is not very satisfactory, but at higher frequencies it follows better the experimental result. On the contrary, the results obtained by decoupling the added mass, modeled as three lumped masses, show a better agreement with the experimental FRFs at low frequencies. However, at low frequencies the two substructures have an almost independent dynamic behavior and at such frequencies the effect of coupling is not very interesting. Therefore, the better prediction above 40 Hz provided by the consistent mass model is preferred.

Acknowledgements This research is supported by University of Rome La Sapienza and University of L'Aquila. The authors acknowledge the dynamic substructuring group of UW-Madison for sharing the results of experimental tests conducted on the Ampair wind turbine test bed on the Wiki site of the Experimental Dynamic Substructuring Focus Group.

References

1. D'Ambrogio W, Sestieri A (2004) A unified approach to substructuring and structural modification problems. *Shock Vib* 11(3–4):295–310
2. Jetmundsen B, Bielawa R, Flannelly W (1988) Generalised frequency domain substructure synthesis. *J Am Helicopter Soc* 33(1):55–64
3. de Klerk D, Rixen DJ, Voormeeren S (2008) General framework for dynamic substructuring: history, review, and classification of techniques. *AIAA J* 46(5):1169–1181
4. de Klerk D (2009) Dynamic response characterization of complex systems through operational identification and dynamic substructuring. Ph.D. thesis, TU Delft
5. D'Ambrogio W, Fregoleto A (2009). In: Decoupling procedures in the general framework of frequency based substructuring. Proceedings of 27th IMAC, Orlando, February 2009
6. D'Ambrogio W, Fregoleto A (2010) The role of interface DoFs in decoupling of substructures based on the dual domain decomposition. *Mech Syst Signal Process* 24(7):2035–2048. doi:10.1016/j.ymssp.2010.05.007, also in Proceedings of ISMA 2010, Leuven, Belgium, pp 1863–1880

7. Voormeeren SN, Rixen DJ (2012) A family of substructure decoupling techniques based on a dual assembly approach. *Mech Syst Signal Process* 27:379–396. doi:10.1016/j.ymssp.2011.07.028
8. Mayes RL (2012) An introduction to the SEM substructures focus group test bed - the Ampair 600 wind turbine. In: Mayes R, Rixen D, Griffith D, De Klerk D, Chauhan S, Voormeeren S, Allen M, Proulx T (eds) *Topics in experimental dynamics substructuring and wind turbine dynamics*, vol 2. Conference proceedings of the Society for Experimental Mechanics series, vol 27. Springer, New York, pp 61–70. doi:10.1007/978-1-4614-2422-2_7
9. Brunetti J, Culla A, D'Ambrogio W, Fregolent A (2014) Selection of interface DoFs in hub-blade(s) coupling of Ampair wind turbine test bed. In: Mayes R, Rixen D, Allen M (eds) *Topics in experimental dynamic substructuring*, vol 2. Conference proceedings of the Society for Experimental Mechanics series. Springer, New York, pp 167–178
10. Culla A, D'Ambrogio W, Fregolent A (2012) Getting a symmetric residue matrix from the poly-reference least square complex frequency domain technique. In: Sas P (ed) *Proceedings of ISMA 2012 - international conference on noise and vibration engineering*, Leuven, Belgium, Sept 2012, pp 2755–2764

Dynamics of Coupled Structures, Volume 1
Proceedings of the 32nd IMAC, A Conference and
Exposition on Structural Dynamics, 2014
Allen, M.; Mayes, R.L.; Rixen, D.J. (Eds.)
2014, IX, 472 p. 377 illus., Hardcover
ISBN: 978-3-319-04500-9